Contrasting thinning patterns between lake- and land-terminating glaciers in the Bhutan Himalaya

Shun Tsutaki[1,a], Koji Fujita[1], Takayuki Nuimura[1,b], Akiko Sakai[1], Shin Sugiyama[2], Jiro Komori[1,3,c], and Phuntsho Tshering[1,3,d]

[1]Graduate School of Environmental Studies, Nagoya University, Nagoya, Japan
[2]Institute of Low Temperature Science, Hokkaido University, Sapporo, Japan
[3]Department of Geology and Mines, Ministry of Economic Affairs, Thimphu, Bhutan
[a]now at: Atmosphere and Ocean Research Institute, The University of Tokyo, Kashiwa, Japan
[b]now at: Chiba Institute of Science, Choshi, Japan
[c]now at: Department of Modern Life, Teikyo Heisei University, Tokyo, Japan
[d]now at: Cryosphere Services Division, National Center for Hydrology and Meteorology, Thimphu, Bhutan

Correspondence: Shun Tsutaki (tsutshun@frontier.hokudai.ac.jp)

Abstract. Despite the importance of glacial lake development in ice dynamics and glacier thinning, in situ and satellite based measurements from lake-terminating glaciers are sparse in the Bhutan Himalaya, where a number of supraglacial lakes exist. To better understand the influences of glacial lake formation and expansion on ice dynamics and glacier thinning, we acquired in situ and satellite based observations across lake- and land-terminating debris-covered glaciers in the Lunana region, Bhutan Himalaya. A repeat differential GPS survey reveals that thinning of the debris-covered ablation area of the lake-terminating Lugge Glacier for the 2004–2011 period (-4.67 ± 0.02 m a^{-1}) is more than three times greater than that of the land-terminating Thorthormi Glacier (-1.40 ± 0.02 m a^{-1}). The surface flow velocity decreases down-glacier along Thorthormi Glacier, whereas it increases from the upper part of ablation area to the terminus of Lugge Glacier. Numerical experiments with a two-dimensional ice flow model demonstrate that the rapid thinning of Lugge Glacier is driven primarily by a negative surface mass balance and that the dynamically induced change in ice thickness is small. However, the thinning of Thorthormi Glacier is suppressed by a longitudinally compressive flow regime. The magnitude of dynamic ice thickening more than offsets the glacier thinning, suggesting that over half of the negative surface mass balance is counterbalanced by the ice dynamics of Thorthormi Glacier. Multiple ponds on Thorthormi Glacier have been expanding since 2000 and merged into a single proglacial lake, with the glacier terminus detaching from its terminal moraine in 2011. Numerical experiments suggest that the speed up and thinning of Thorthormi Glacier will be accelerated with continued proglacial lake development.

1 Introduction

The spatially heterogeneous shrinkage of Himalayan glaciers has been revealed by in situ measurements (Yao et al., 2012; Azam et al., 2018), satellite based observations (Bolch et al., 2012; Kääb et al., 2012; Brun et al., 2017), mass balance and climate models (Fujita and Nuimura, 2011; Mörg et al., 2014), and a compilation of multiple methods (Cogley, 2016). Glaciers in Bhutan in the southeastern Himalayas have experienced significant shrinkage and thinning over the past four decades. For

example, the Bhutanese glaciers shrank by 23.3 ± 0.9 % between the 1980s and 2010, based on repeated decadal glacier inventories (Bajracharya et al., 2014). Multitemporal digital elevation models (DEMs) revealed that the ice thinning rate in the ablation area of Bhutanese glaciers was 0.17 ± 0.05 m w.e. a^{-1} during 1974–2006 (Maurer et al., 2016) and 0.22 ± 0.12 m w.e. a^{-1} during 1999–2010 (Gardelle et al., 2013). Bhutanese glaciers are inferred to be sensitive to changes in air temperature and pre-

25 cipitation, because they are affected by monsoon influenced humid climate conditions (Fujita, 2008; Sakai and Fujita, 2017). Tshering and Fujita (2016) reported a mass balance record of Gangju La Glacier in the central Bhutan Himalaya between 2003 and 2014, based on in situ measurements, where the glacier experienced much greater mass loss than neighbouring glaciers in the eastern Himalaya and southeastern Tibet. It is therefore crucial to investigate the mass loss of Bhutanese glaciers to advance our understanding of their mechanisms, to provide more accurate analyses of regional water availability (Immerzeel

30 et al., 2010) and improve projections of global sea level rise and glacier evolution (Huss and Hock, 2015).

  In recent decades, glacial lakes have formed and expanded at the termini of retreating glaciers in the Himalayas (Ageta et al., 2000; Komori, 2008; Fujita et al., 2009; Hewitt and Liu, 2010; Sakai and Fujita, 2010; Gardelle et al., 2011; Nie et al., 2017). Such proglacial lakes are dammed by terminal and lateral moraines, or stagnant ice masses at the glacial front (Sakai, 2012; Carrivick and Tweed, 2013). The formation and expansion of proglacial lakes accelerates glacier retreat through flotation

35 of the terminus, increased calving, and ice flow (e.g., Funk and Röthlisberger, 1989; Warren and Kirkbride, 2003; Tsutaki et al., 2013). The ice thinning rates of lake-terminating glaciers are generally greater than those of neighbouring land-terminating glaciers in the Nepal and Bhutan Himalayas (Nuimura et al., 2012; Gardelle et al., 2013; Maurer et al., 2016; King et al., 2017). Increases in ice discharge and flow velocity at the glacier terminus cause rapid thinning due to longitudinal stretching, known as dynamic thinning. For example, dynamic thinning accounted for 17 % of the total ice thinning at lake-terminating Yakutat

40 Glacier, Alaska, during 2007–2010 (Trüssel et al., 2013). Therefore, it is important to quantify the contributions of dynamic thinning and surface mass balance (SMB) to evaluate ongoing mass loss and predict the future evolution of lake-terminating glaciers in Bhutan.

  To investigate the contribution of dynamically induced changes in ice thickness to glacier thinning, it is beneficial to compute the ice flow field of a lake-terminating glacier using an ice flow model. Two-dimensional ice flow models have been utilized

45 to investigate the dynamic thinning of marine-terminating outlet glaciers (Benn et al., 2007a; Vieli and Nick, 2011), which require the ice flow velocity and glacier thickness. In Bhutan, ice flow velocity measurements have been carried out via remote sensing techniques with optical satellite images (Kääb, 2005; Bolch et al., 2012; Dehecq et al., 2015) and by in situ GPS surveys (Naito et al., 2012), but no ice thickness data are available. Another approach to investigate the relative importance of ice dynamics in glacier thinning is to compare lake- and land-terminating glaciers in the same region. This method has been

50 applied to neighbouring lake- and land-terminating glaciers in Nepal and other regions (Nuimura et al., 2012; Trüssel et al., 2013; King et al., 2017).

  Widespread thinning of Himalayan glaciers has been revealed by differencing multitemporal DEMs constructed from satellite image photogrammetry (e.g., Gardelle et al., 2013; Maurer et al., 2016; Brun et al., 2017). However, the accuracy of the remotely sensed DEMs is still insufficient to measure several metres of glacier elevation change. Repeated differential GPS

55 measurements, which are acquired with sub metre accuracy, enable us to evaluate elevation changes of several metres (e.g.,

Fujita et al., 2008). Although their temporal and spatial coverage is limited, repeated differential GPS measurements have been successfully performed to investigate glacier surface elevation change in Bhutan (Tshering and Fujita, 2016), Nepal (Vincent et al., 2016), and the Inner Tien Shan (Fujita et al., 2011).

To investigate the importance of glacial lake formation and expansion on rapid glacier thinning, we measured surface elevation changes on lake- and land-terminating glaciers in the Lunana region, Bhutan Himalaya. Following a previous report of surface elevation measurements from a differential GPS survey (Fujita et al., 2008), we repeated the differential GPS survey on the lower parts of the land-terminating Thorthormi and Lugge II glaciers, as well as the adjacent lake-terminating Lugge Glacier. Thorthormi and Lugge glaciers were selected for analysis because these glaciers are situated around the same elevation, thus making them suitable for evaluating the contribution of dynamic thinning to the observed ice thickness changes. We also performed numerical simulations to evaluate the contributions of SMB and dynamic thinning to the surveyed glacier thinning.

2 Study site

This study focuses on three debris-covered glaciers (Thorthormi, Lugge, and Lugge II) in the Lunana region of northern Bhutan (Fig. 1a, 28°06' N, 90°18' E). Thorthormi Glacier covers an area of 13.16 km^2, based on a satellite image from 17 January 2010 (Table S1 in the Supplement, Nagai et al., 2016). The ice flows to the south in the upper part and to the southwest in the terminal part of the glacier at rates of 60–100 m a^{-1} (Bolch et al., 2012). The surface is almost flat ($< 1°$) within 3000 m of the glacier terminus. The glacier thinned at a rate of -3 m a^{-1} during the 2000–2010 period (Gardelle et al., 2013). A large supraglacial lake, which is inferred to possess a high potential for outburst flood (Fujita et al., 2008, 2013), formed on the western ablation area by the merging of multiple supraglacial ponds (Ageta et al., 2000; Komori, 2008). In 2011, the glacier terminus was in contact with the terminal moraine, and thus Thorthormi Glacier was a land-terminating glacier. Lugge Glacier is a lake-terminating glacier with an area of 10.93 km^2 in May 2010 (Table S1, Nagai et al., 2016). The mean surface slope is 12° within 3000 m of the glacier terminus. A moraine dammed proglacial lake has expanded since the 1960s (Ageta et al., 2000; Komori, 2008), and the glacier terminus retreated by ~ 3000 m during 1980–2010 (Bajracharya et al., 2014). Lugge Glacier thinned near the terminus at a rate of -8 m a^{-1} during 2000–2010 (Gardelle et al., 2013). On 7 October 1994, an outburst flood, with a volume of 17.2×10^6 m^3, occurred from Lugge Glacial Lake (Fujita et al., 2008). The depth of Lugge Glacial Lake was 126 m at its deepest location, with a mean depth of 50 m, based on a bathymetric survey in September 2002 (Yamada et al., 2004). Lugge II Glacier is a land-terminating glacier with an area of 3.18 km^2 in January 2010 (Table S1, Nagai et al., 2016), whose terminus retreated by < 200 m from 1980 to 2010 (Bajracharya et al., 2014). The mean surface slope is 15° within 3000 m of the glacier terminus. The mean thinning rate over the entire glacier was ~ 1 m a^{-1} during 2000–2010 (Gardelle et al., 2013).

Meteorological and glaciological in situ observations were carried out on/around the glaciers and lakes in the Lunana region from 2002 to 2004 (Yamada et al., 2004). Automatic weather station (AWS) observations from the terminal moraine of Lugge Glacial Lake (4524 m a.s.l., Fig. 1a) showed that the annual mean air temperature during 2002–2004 was ~ 0 °C, and annual

precipitation in 2003 was 900 mm (Suzuki et al., 2007b). Naito et al. (2012) reported changes in surface elevation and ice

90 flow velocity along the central flowline in the lower parts of Thorthormi and Lugge glaciers for the period 2002–2004. The ice thinning rate at Lugge Glacier was $\sim$ 5 m a^{-1} during 2002–2004, which is much higher than that at Thorthormi Glacier (0–3 m a^{-1}). The ice flow velocity across Thorthormi Glacier decreases down-glacier from $\sim$ 90 to $\sim$ 30 m a^{-1} at 2000–3000 m from the terminus, while the ice flow velocity of Lugge Glacier is nearly uniform at 40–55 m a^{-1} within 1500 m of the terminus (Naito et al., 2012).

3 Data and methods

3.1 Surface elevation change

We surveyed the surface elevations in the lower parts of Thorthormi, Lugge, and Lugge II glaciers from 19 to 22 September 2011, and then compared them with those observed from 29 September to 10 October 2004 (Fujita et al., 2008). We used dual- and single-frequency carrier phase GPS receivers (GNSS Technologies, GEM-1, and MAGELLAN ProMark3). One receiver

100 was installed 2.5 km west of the terminus of Thorthormi Glacier as a reference station, whose location was determined by an online precise point positioning processing service (https://webapp.geod.nrcan.gc.ca/geod/tools-outils/ppp.php?locale=en, last accessed: 19 January 2018), which provided standard deviations of < 4 mm for both the horizontal and vertical coordinates after one week of continuous measurements in 2011. Observers walked on/around the glaciers with a GPS receiver and antenna fixed to a frame pack. The height uncertainty of the GPS antenna during the survey was < 0.1 m (Tsutaki et al., 2016). The

105 GPS data were processed with RTKLIB, an open source software for GNSS positioning (http://www.rtklib.com/, last accessed: 19 January 2018). Coordinates were projected onto a common Universal Transverse Mercator projection (UTM zone 46N, WGS84 reference system). We generated DEMs with 1 m resolution by interpolating the surveyed points with an inverse distance weighted method, as used in previous studies (e.g., Fujita and Nuimura, 2011; Tshering and Fujita, 2016). The 2004 survey data were calibrated with four benchmarks around the glaciers (Fig. 1a) to generate a 1 m resolution DEM. Details of

110 the 2004 and 2011 GPS surveys, along with their respective DEMs, are summarized in Table S1. The surface elevation changes between 2004 and 2011 were computed at points where data were available for both dates. Elevation changes were obtained at 431, 248, and 258 DEM grid points for Thorthormi, Lugge and Lugge II glaciers, respectively (Table 1).

The horizontal uncertainty of the GPS survey was evaluated by comparing the positions of four benchmarks installed around Lugge and Thorthormi glaciers (Fig. 1a). We evaluated the vertical uncertainty (σ_e) from the off glacier elevation difference

115 between the 2004 and 2011 DEMs ($n = 3893$, Table 1), which was calculated as the quadratic sum of the mean elevation difference (dZ) and standard deviation (σ_Z) (Bolch et al., 2011). In previous studies, the vertical uncertainty in differentiation of two satellite based DEMs has been expressed by the standard error (σ_{se}) as follows:

$$\sigma_{se} = \frac{\sigma_e}{\sqrt{n}}. \tag{1}$$

The number of DEM grid points over a glacier is generally used as the sample number (e.g., Berthier et al., 2007; Bolch et al.,

120 2011; Maurer et al., 2016).

3.2 Surface flow velocity

We calculated the surface flow velocities by processing ASTER images (15 m resolution, near infrared (NIR), near nadir 3N band) with the COSI-Corr feature tracking software (Leprince et al., 2007), which is commonly adopted in mountainous terrain to measure surface displacements with an accuracy of one-fourth to one-tenth of the pixel size (e.g., Heid and Kääb, 2012; Scherler and Strecker, 2012; Lamsal et al., 2017). Orthorectification and coregistration of the images were performed by Japan Space Systems before processing. We selected five image pairs from seven scenes between 22 October 2002 and 12 October 2010, with temporal separations ranging from 273 to 712 days (Table S2), to obtain annual surface flow velocities of the glaciers. It should be noted that the aim of our flow velocity measurements is to investigate the mean surface flow regime of the glaciers rather than its interannual variability. The subpixel displacement of features on the glacier surface was recorded at every fourth pixel in the orthorectified ASTER images, providing the horizontal flow velocity at a 60 m resolution (Scherler et al., 2011). We used a statistical correlation mode, with multiscale window sizes of 16×16 pixels (Leprince et al., 2007). The obtained ice velocity fields were filtered to remove residual attitude effects and miscorrelations (Scherler et al., 2011; Scherler and Strecker, 2012). The filters eliminated those flow vectors showing a large deviation in magnitude ($> 1\ \sigma$) or direction ($> 20°$) relative to the mean of the neighbouring 21×21 data points.

3.3 Glacier area

We analysed the aerial variations in the ablation area of Thorthormi and Lugge glaciers using 12 satellite images acquired by the Landsat 7 ETM+ between November 2000 and December 2011 (distributed by the United States Geological Survey, http://landsat.usgs.gov/, last accessed: 19 January 2018). We selected images taken in either November or December that possessed the least snow and cloud cover. The lowermost 4000 m of Thorthormi Glacier and the lowermost 2000 m of Lugge Glacier were manually delineated on false colour composite images (bands 3–5, 30 m spatial resolution) using the QGIS geographical information system software (http://qgis.org/en/site/, last accessed: 19 January 2018). For Thorthormi Glacier, supraglacial ponds surrounded by ice were included in the glacier surface, whereas marginal ponds in contact with bedrock/moraine ridge were excluded. The accuracy of the outline mapping is equivalent to the image resolution (30 m). The coregistration error in the repeated images was ± 30 m, based on visual inspection of the horizontal shift of a stable bedrock and lateral moraines on the coregistered imagery. The total error of the area analysis was ± 0.002 km^2 ($\sqrt{30^2 + 30^2}^2 = 1800$ m^2).

3.4 Mass balance of the debris-covered surface

SMB is an essential component of ice thickness change, but no in situ SMB data are available in the Lunana region. Therefore, the spatial distributions of the SMB on the debris-covered Thorthormi, Lugge, and Lugge II glaciers were computed with a heat and mass balance model, which quantifies the spatial distribution of the mean SMB for each glacier.

Thin debris accelerates ice melt by lowering surface albedo, while thick debris (generally more than a few centimetres) suppresses ice melt and acts as an insulating layer (Østrem, 1959; Mattson et al., 1993). To obtain the spatial distributions of debris thickness and SMB, we calculated the thermal resistance from remotely sensed data and reanalysis climate data (Suzuki

et al., 2007a; Zhang et al., 2011; Fujita and Sakai, 2014). The thermal resistance (R_T, m^2 K W^{-1}) is defined as follows:

$$R_T = \frac{h}{\lambda}, \tag{2}$$

155   where h and λ are the debris thickness (m) and thermal conductivity (W m^{-1} K^{-1}), respectively. This method has been applied to reproduce debris thickness and SMB in southeastern Tibet (Zhang et al., 2011) and glacier runoff in the Nepal Himalaya (Fujita and Sakai, 2014). Using eight ASTER images obtained between October 2002 and October 2010 (Table S3), along with the NCEP/NCAR reanalysis climate data (NCEP-2, Kanamitsu et al., 2002), we calculated the distribution of mean thermal resistance on the three target glaciers. The uncertainty in thermal resistance was evaluated as 64 % by taking the standard

160   deviations calculated from multiple images at the same location (Fig. S1 in the Supplement).

The SMB of the debris-covered ablation area was calculated by a heat and mass balance model that included debris-covered effects (Fujita and Sakai, 2014). By assuming no heat storage, a linear temperature profile within a debris layer, and the melting point temperature at the ice–debris interface (T_i, 0 °C), the conductive heat flux through the debris layer (G_d, W m^{-2}) and the heat balance at the debris surface are described as follows:

165    $$G_d = \frac{(T_s - T_i)}{R_T} = (1 - \alpha_d)R_{Sd} + R_{Ld} - R_{Lu} + H_S + H_L, \tag{3}$$

where α_d is the debris surface albedo; R_{Sd}, R_{Ld}, and R_{Lu} are the downward short wave radiation, and downward and upward long wave radiation, respectively (positive sign, W m^{-2}); and H_S and H_L are the sensible and latent heat fluxes (W m^{-2}), respectively, which are positive when the fluxes are directed toward the ground. The surface temperature is determined to satisfy Eq. (3) using an iterative calculation, and then, if the heat flux toward the ice–debris interface is positive, the daily

170   amount of ice melt beneath the debris mantle (M_d, kg m^{-2} d^{-1}) is obtained as follows:

$$M_d = \frac{t_D G_d}{l_m}, \tag{4}$$

where t_D is the length of a day in seconds (86400 s) and l_m is the latent heat of fusion of ice (3.33×10^5 J kg^{-1}). Snow accumulation was neglected in the model, because snow on the debris surface melted immediately on the studied glaciers. Further detailes on the equations and methodology used in this study are described by Fujita and Sakai (2014). The mass

175   balance was calculated at 90×90 m mesh grid points on the debris-covered ablation area of the three glaciers using two years of in situ meteorological data (2002–2004) from the terminal moraine of Lugge Glacier (Fig. 1a, Suzuki et al., 2007b), with the results given in metres of water equivalent (w.e.).

3.5   Ice dynamics

3.5.1   Model descriptions

180   To investigate the dynamically induced ice thickness change, numerical experiments were carried out by applying a two-dimensional ice flow model to the longitudinal cross sections of Thorthormi and Lugge glaciers. The aim of the experiments was to investigate whether the ice thickness changes observed at Thorthormi and Lugge glaciers were affected by the presence of proglacial lakes.

The model was developed for a land-terminating glacier (Sugiyama et al., 2003, 2014), and is applied to the lake-terminating

185 glaciers in this study. Taking the x and z coordinates in the along flow and vertical directions, the momentum and mass conservation equations in the x–z plane are

$$\frac{\partial \sigma_{xx}}{\partial_x} + \frac{\partial \sigma_{xz}}{\partial_z} = 0, \tag{5}$$

$$\frac{\partial \sigma_{zx}}{\partial_x} + \frac{\partial \sigma_{zz}}{\partial_z} = \rho_i g, \tag{6}$$

190

$$\frac{\partial u_x}{\partial_x} + \frac{\partial u_z}{\partial_z} = 0, \tag{7}$$

where σ_{ij} ($i, j = x, z$) are the components of the Cauchy stress tensor, ρ_i is the density of ice (910 kg m^{-3}), g is the vertical component of the gravitational acceleration vector (9.81 m s^{-2}), and u_x and u_z are the horizontal and vertical components of the velocity vector, respectively. The stress in Eq. (6) and Eq. (7) is linked to the strain rate via the constitutive equation given

195 by Glen's flow law (Glen, 1955):

$$\dot{\epsilon}_{ij} = A\tau_e^{n-1}\tau_{ij}, \tag{8}$$

where $\dot{\epsilon}_{ij}$ and τ_{ij} are the components of the strain rate and deviatoric stress tensors, respectively, and τ_e is the effective stress, which is described as

$$\tau_e = \frac{1}{2}(\tau_{xx}^2 + \tau_{zz}^2) + \tau_{xz}^2. \tag{9}$$

200 The rate factor (A) and flow law exponent (n) are material parameters. We used the commonly accepted value of $n = 3$ for the flow law exponent, and employed a rate factor of $A = 75$ MPa^{-3} a^{-1}, which was previously used for modelling a temperate valley glacier (Gudmundsson, 1999).

The model domain was within 5100 m and 3500 m of the termini of Thorthormi and Lugge glaciers, respectively. The surface geometry was obtained from ASTER GDEM version 2 after filtering the elevations with a smoothing routine at a bandwidth

205 of 1000 m. The ice thickness distribution was estimated from a method proposed for alpine glaciers (Farinotti et al., 2009). We applied the same local regression filter to smooth the estimated bedrock geometry. The bedrock elevation of Thorthormi Glacier was estimated from bathymetry data acquired in September 2011 at 1400 m from the terminus (Fig. 6a). For Lugge Glacier, the bed elevation at the glacier front was estimated from the bathymetric map of Lugge Glacial Lake, surveyed in September 2002 (Fig. 6b, Yamada et al., 2004). To solve Eq. (6) and Eq. (7) for u_x and u_z, the modelled domain was discretized with a

210 finite element mesh. The mesh resolution was 100 m in the horizontal direction, and several metres near the bed and 10–28 m near the surface in the vertical direction. The total numbers of elements were 612 and 420 for Thorthormi and Lugge glaciers, respectively (Figs. 6a and 6b).

The upper surface of the domain was assumed to be stress free. The ice flux through the upper boundary was prescribed according to the measured surface flow velocities. The basal sliding velocity (u_b) was given as a linear function of the basal

215   shear traction ($\tau_{xz,b}$):

$$u_b = C\tau_{xz,b}, \tag{10}$$

where C is the sliding coefficient. We used constant sliding coefficients of $C = 766$ and 125 m a^{-1} MPa^{-1} over the entire domains of Thorthormi and Lugge glaciers, respectively. These parameters were obtained by minimizing the RMSE between the modelled and measured surface flow velocities over the entire model domains (Fig. S2).

220   ### 3.5.2   Experimental configurations

To quantify the effect of glacier dynamics on ice thickness change, we performed two experiments for Thorthormi and Lugge glaciers. Experiment 1 was performed to compute the ice flow velocity fields under the present terminus conditions. In this experiment, Thorthormi Glacier was treated as a land-terminating glacier by prescribing zero horizontal velocity at the glacier front, whereas Lugge Glacier was treated as a lake-terminating glacier by applying hydrostatic pressure at the front as a function

225   of water depth. A stress-free boundary condition was given to the calving front above the lake level.

Experiment 2 was designed to investigate the influence of proglacial lakes on glacier dynamics. For Thorthormi Glacier, we assumed a calving front with thickness of 106 m (Fig. 7a). The surface level of the proglacial lake was assumed to be 4432 m a.s.l., which is the mean surface level of the supraglacial ponds measured in September 2004 (Fujita et al., 2008). Hydrostatic pressure and stress-free conditions were applied to the lower boundary below and above the lake level, respectively.

230   For Lugge Glacier, the present 2200 m long Lugge Glacial Lake is filled with ice, so that the glacier terminates on land. Bedrock topography is derived from the bathymetric map (Fig. 7b, Yamada et al., 2004). The surface topography is linearly extrapolated from the surface elevations at the calving front in 2002, and zero velocity was assumed at the terminus. In the experiment, we used 444 and 684 elements for Thorthormi and Lugge glaciers, respectively (Figs. 7a and 7b).

4   Results

235   ### 4.1   Surface elevation change

Figure 1a shows the rate of surface elevation change of Thorthormi, Lugge, and Lugge II glaciers from 2004 to 2011. The rates for Thorthormi Glacier range from -3.37 to $+1.14$ m a^{-1}, with a mean rate of -1.40 m a^{-1} (Table 1). The rates show large variability within the limited elevation band (4410–4450 m a.s.l., Fig. 2b). No clear trend is observed at 1000–3000 m from the terminus (Fig. 2c). The rates for Lugge Glacier range from -9.13 to -1.30 m a^{-1}, with a mean rate of -4.67 m a^{-1} (Table 1).

240   The most negative values (-9 m a^{-1}) are found in the lower elevation band (4560 m a.s.l., Fig. 2b), which corresponds to 1300 m from the 2002 terminus position (Fig. 2c). The rates of surface elevation change for Lugge II Glacier range from -3.99 to $+0.10$ m a^{-1}, with a mean rate of -0.63 m a^{-1} (Table 1).

The RMSE between the surveyed positions (five measurements in total, with one or two measurements for each benchmark) is 0.21 m in the horizontal direction. The mean elevation difference between the 2004 and 2011 DEMs (dZ) is 0.48 m, with
245   a standard deviation (σ_Z) of 1.91 m (Fig. 2a) and a vertical uncertainty (σ_e) of 1.97 m (0.28 m a^{-1}). According to Eq. (1), the standard error for this study ranges from 0.09 to 0.12 m (< 0.02 m a^{-1}), while those for the remotely sensed studies of Himalayan glaciers have been evaluated at 1.1–6.4 m (e.g., Berthier et al., 2007; Bolch et al., 2011; Maurer et al., 2016), suggesting that our data are considerably more accurate than those reported in the aforementioned studies.

4.2   Surface flow velocity

250   Figure 1b shows the surface flow velocity field from 30 January 2007 to 1 January 2008 (337 days). On Thorthormi Glacier, the flow velocity decreases down-glacier, ranging from ~ 110 m a^{-1} at the foot of the icefall to < 10 m a^{-1} at the terminus (Fig. 3a). The flow velocity of Lugge Glacier increases down-glacier, ranging from 20–60 to 50–80 m a^{-1} within 2000 m of the calving front (Fig. 3b). In this region, the ice flow converges as the glacier width narrows down-glacier. Lugge II Glacier flows more slowly than the other two glaciers, typically at < 40 m a^{-1} across the entire glacier (Fig. 3c).

255   The surface flow velocity of Thorthormi Glacier shows little variability from 2002–2003 to 2009–2010. The only exception is at 900–1200 m from the terminus, where the velocity increased by ~ 20 m a^{-1} from 2002–2003 to 2007–2008 (Fig. 3a). The flow velocity of Lugge Glacier showed no significant change between 2002–2003 and 2008–2009. The glacier then decelerated in 2009–2010 at 500–2000 m from the terminus (Fig. 3b). No clear temporal variation was observed at Lugge II Glacier (Fig. 3c).

260   Uncertainties in the flow velocity were ~ 5 m a^{-1}, as given by the mean off glacier displacement from 3 February 2006 to 30 January 2007 (0.99 years). Scherler and Strecker (2012) applied the same procedures to Biafo Glacier in Karakoram with ASTER images and obtained an uncertainty of 1–5 m a^{-1} for timespans of 1–3 years. Thus, our velocity calculations are of the same quality as those reported by Scherler and Strecker (2012).

4.3   Changes in glacier terminus

265   Thorthormi Glacier progressively shrank in size from 2000 to 2010, at a mean rate of -0.09 km^2 a^{-1} and accelerated loss between 2010 and 2011 (-0.49 km^2 a^{-1}) (Figs. 4a and 5). This change was due to the rapid retreat of the northern half of the glacier front by 200–1400 m. Lugge Glacier also shrank in size from 2000 to 2011, at a mean rate of -0.03 km^2 a^{-1} (Figs. 4b and 5). Since 2009, the calving front has retreated more rapidly along the northern half of the glacier front (by 300–400 m) than along the southern half (by < 200 m) (Fig. 4b). The total area changes from 2000 to 2011 are -1.40 km^2 for Thorthormi
270   Glacier and -0.33 km^2 for Lugge Glacier.

4.4   Mass balance of the debris-covered surface

The simulated SMB shows a spatially heterogeneous distribution among the three glaciers (Fig. 1c). For example, the debris-free surface along the centre of Thorthormi Glacier shows more negative SMB (-7.5 to -8.5 m w.e. a^{-1}) than the debris-

covered regions (-5.0 to -7.0 m w.e. a^{-1}, Fig. 1c). The SMB is more uniformly distributed within 2000 m of the calving

275 front of Lugge Glacier, on both the debris-free (-6.0 to -7.5 m w.e. a^{-1}) and debris-covered (-5.5 to -7.0 m w.e. a^{-1}) surfaces. The SMB of Lugge II Glacier is significantly less negative than those of other two glaciers, ranging from -5.5 to $+0.0$ m w.e. a^{-1} (Fig. 2b). Over the studied area, the mean SMB is -7.9, -6.0, and -4.4 m w.e. a^{-1} for Thorthormi, Lugge, and Lugge II glaciers, respectively (Table 1).

4.5 Numerical experiments of ice dynamics

280 The ice thinning of Lugge Glacier was three times faster than that of Thorthormi Glacier. However, the mean SMB was 1.3 times more negative at Thorthormi Glacier, suggesting a substantial influence of glacier dynamics on ice thickness change. To quantify the contribution of ice dynamics to the ice thickness change, we performed numerical experiments with the present (Experiment 1) and prescribed (Experiment 2) glacier geometries.

4.5.1 Experiment 1 – present geometry

285 Modelled results for the present geometry show significantly different flow velocity fields for Thorthormi and Lugge glaciers (Figs. 6c and 6d). Thorthormi Glacier flows faster (> 150 m a^{-1}) in the upper reaches, where the surface is steeper than the other regions (Fig. 6c). Down-glacier of the icefall, where the glacier surface is flatter, the ice motion slows in the down-glacier direction, with the velocities decreasing to < 10 m a^{-1} near the terminus (Fig. 6e). Ice flows upward relative to the surface across most of the modelled region (Fig. 6c). In contrasted to the observed decrease in the velocity at Thorthormi, the computed

290 velocities of Lugge Glacier gradually increase down-glacier, up to ~ 40 m a^{-1}, and then sharply increase to ~ 80 m a^{-1} at the calving front (Fig. 6f). Ice flow is nearly parallel to the glacier surface, except for the more downward motion near the calving front (Fig. 6d). Within 3000 m of the terminus of Thorthormi Glacier, the modelled surface flow velocities are in good agreement with the satellite derived velocities (Fig. 6e). The calculated surface velocities of Lugge Glacier are within 7 % of the satellite derived velocities (Fig. 6f).

295 4.5.2 Experiment 2 – contrasting geometry

Figure 7c shows the flow velocities simulated for the lake-terminating boundary condition of Thorthormi Glacier, in which the flow velocities within 200 m of the calving front are three to four times faster than those of Experiment 1 (Figs. 6c and 7c). The mean vertical surface flow velocity within 2000 m of the front is still positive (0.9 m a^{-1}), but is smaller than that for the land-terminating condition (1.6 m a^{-1}). The modelled result demonstrates significant acceleration as the glacier dynamics change

300 from a compressive to stretching flow regime after proglacial lake formation. For Lugge Glacier, the flow velocity decreases over the entire glacier in comparison with Experiment 1 (Figs. 6d and 7d). The upward ice motion appears within 3000 m of the terminus. The numerical experiments demonstrate that the formation of a proglacial lake causes significant changes in ice dynamics.

5 Discussion

5.1 Glacier thinning

305

The repeated GPS surveys revealed rapid thinning of Lugge Glacier between 2004 and 2011. The mean rate of surface elevation change (-4.67 ± 0.02 m a^{-1}) is comparable to that for the 2002–2004 period (-5 m a^{-1}, Naito et al., 2012). Gardelle et al. (2013) reported the rates of surface elevation change ranging from -8 to -3 m a^{-1} during 2000–2010, as determined from the differencing of satellite derived DEMs. Lugge Glacier is thinning more rapidly than neighbouring glaciers in the

310 Nepal and Bhutan Himalayas. The mean rate of surface elevation change was -0.50 ± 0.14 m a^{-1} in the ablation area of Bhutanese glaciers for the period 2000–2010 (Gardelle et al., 2013), and -2.30 ± 0.53 m a^{-1} for debris-free glaciers in eastern Nepal and Bhutan during 2003–2009 (Kääb et al., 2012). Maurer et al. (2016) reported that the mean thinning rate for Lugge Glacier during 1974–2006 (-0.6 ± 0.2 m a^{-1}) was greater than those for other Bhutanese lake-terminating glaciers (-0.2 to -0.4 m a^{-1}). The rate of surface elevation change of Thorthormi Glacier (from -3.37 to $+1.14$ m a^{-1} from 2004

315 to 2011) is comparable with previous measurements, which range from -3 to 0 m a^{-1} for the period 2002–2004 (Naito et al., 2012) and from -3 to 0 m a^{-1} during 2000–2010 (Gardelle et al., 2013). The mean rate across Thorthormi Glacier was -0.3 ± 0.2 m a^{-1} during 1974–2006 (Maurer et al., 2016), which is a typical rate in the Bhutan Himalaya.

Lugge Glacier thinned more rapidly than Thorthormi and Lugge II glaciers, which is consistent with previous satellite based studies. For example, the thinning rates of the lake-terminating Imja and Lumding glaciers (-1.14 and -3.41 m a^{-1},

320 respectively) were greater than those of the land-terminating glaciers (approximately -0.87 m a^{-1}) in the Khumbu region of the Nepal Himalaya (Nuimura et al., 2012). King et al. (2017) measured the thinning of the lower parts of nine lake-terminating glaciers in the Everest area (approximately -2.5 m a^{-1}), which was faster than that of 18 land-terminating glaciers (approximately -1.5 m a^{-1}). The lake-terminating glaciers in Yakutat ice field, Alaska, thinned at a rate of -4.76 m a^{-1}, which was $\sim 30\%$ greater than the neighbouring land-terminating glaciers (Trüssel et al., 2013). It should be noted that the difference

325 in thinning rate between Lugge and Thorthormi glaciers (3.3 times) is much greater than the numbers previously reported in the Nepal Himalaya, suggesting that ice dynamics play a more significant role here.

Glacier thinning has accelerated in recent decades, particularly in the lower parts of Lugge and Thorthormi glaciers. For example, the mean rates of elevation change over Lugge (-4.67 ± 0.02 m a^{-1}) and Thorthormi (-1.40 ± 0.01 m a^{-1}) are more negative than those reported for the 1974–2006 period (-1.7 ± 0.2 m a^{-1} for Lugge and -0.9 ± 0.2 m a^{-1} for

330 Thorthormi, Maurer et al., 2016). These changes are consistent with the accelerating mass loss of glaciers in northern Bhutan. Regional mass balances in northern Bhutan have accelerated from -0.17 ± 0.05 m w.e. a^{-1} for 1974–2006 (Maurer et al., 2016) to -0.22 ± 0.12 m w.e. a^{-1} for 1999–2011 (Gardelle et al., 2013), to -0.42 ± 0.20 m w.e. a^{-1} for 2000–2016 (Brun et al., 2017), and -0.52 ± 0.16 m w.e. a^{-1} for 2003–2008 (Kääb et al., 2012). The mass change of Bhutanese glaciers is expected to be sensitive to precipitation, which varies under the influence of the summer monsoon (Fujita and Ageta, 2000;

335 Fujita, 2008). The summer monsoon has been weakening since the 1950s (Bollasina et al., 2011), which might have reduced the amount of snowfall across the present study area. This trend is likely one of the reasons for the accelerated glacier thinning in recent years. However, care should be taken in making such inferences because previous studies covered different spatial

extents, used different methods to fill data gaps in the accumulation zones, and suffered from uncertainties in SRTM data due

to radar penetration (Zemp et al., 2015; Maurer et al., 2016). Regardless, the thinning rate increased by a greater amount at

340 Lugge Glacier than at Thorthormi Glacier from 1974–2006 to 2004–2011, indicating that the rapid thinning of Lugge Glacier

is affected by a change in ice dynamics. A likely interpretation is that dynamic thinning was enhanced by glacier acceleration

after the expansion of Lugge Glacial Lake in the 1960s.

5.2 Influence of ice dynamics on glacier thinning

The SMB of Lugge Glacier for the 2002–2004 period (-5.98 ± 1.11 m w.e. a^{-1}) is 1.3 times more negative than its thinning

345 rate for the 2004–2011 period (-4.25 ± 0.02 m w.e. a^{-1}), which is converted to water equivalent using an ice density of

910 kg m^{-3}, while the negative SMB of Thorthormi Glacier (-7.87 ± 1.46 m w.e. a^{-1}) is 6.2 times more negative than its

thinning rate (-1.27 ± 0.01 m w.e. a^{-1}). This result suggests that the rapid thinning is due mainly to surface melting along

Lugge Glacier, whereas the negative SMB is counterbalanced by the vertical straining of Thorthormi Glacier (Figs. 6c and

6d). The horizontal flow velocity of Lugge Glacier is nearly uniform along the central flowline, with ice flow parallel to the

350 glacier surface (Fig. 6d), suggesting that the dynamically induced change in ice thickness is small. However, the flow velocity

of Thorthormi Glacier decreases toward the terminus (Fig. 6c), resulting in thickening under a longitudinally compressive flow

regime. To compare the influence of ice dynamics on glacier thinning in lake- and land-terminating glaciers, we calculated the

emergence velocity (v_e) as follows:

$$v_e = (v_z - v_h \tan \alpha) \frac{\rho_i}{\rho_w}, \tag{11}$$

355 where v_z and v_h are vertical and horizontal velocities, respectively, and α is the surface slope (Cuffey and Paterson, 2010).

The emergence velocity is converted into water equivalent (m w.e. a^{-1}), using the densities of ice (ρ_i, 910 kg m^{-3}) and water

(ρ_w, 1000 kg m^{-3}), for comparison with SMB. Figure 8a shows the computed emergence velocity and SMB along the central

flowlines of the glaciers. The emergence velocity of Lugge Glacier ranges from -1.1 to -0.1 m w.e. a^{-1} within 780–1510 m

of the terminus (Fig. 8a), with more negative values near the calving front, at around -10 m w.e. a^{-1} due to the increase in

360 flow velocity toward the glacier front (Fig. 6f). The mean SMB of Thorthormi Glacier is 37 % more negative than that of Lugge

Glacier, which is due to the glacier being situated at lower elevations (Figs. 6a and 6b). The surface elevation change over time

(dh/dt, m a^{-1}), caused by the imbalance of the emergence velocity and SMB along the central flowline, is calculated as

$$\frac{dh}{dt} = (\text{SMB} + v_e) \frac{\rho_w}{\rho_i}. \tag{12}$$

Under the modelled conditions, the rate of elevation change of Lugge Glacier is -6.3 to -7.4 m a^{-1} within 700–1500 m of

365 the calving front, which is ~ 60 % more negative than the observations (Fig. 8b).

In contrast to Lugge Glacier, the emergence velocity of Thorthormi Glacier is positive over the entire model domain. The

emergence velocity ranges from 2.9 to 4.0 m w.e. a^{-1} within 1300–2800 m of the terminus and increases to > 10 m a^{-1} in

the upper reaches (Fig. 8a). The rate of elevation change estimated by Eq. (12) ranges from -4.7 to $+5.0$ m a^{-1} over the in

situ surveyed domain (Fig. 8b). These values agree with the observation at 2400–3200 m from the terminus, falling within

370 the uncertainty range, while they are much more negative than the observation in the lower reaches. The calculated rate of elevation change over the surveyed domain is equivalent to one-third of the SMB, implying that approximately two-thirds of the surface ablation is counterbalanced by ice dynamics. In other words, dynamically induced thickening compensates for the negative SMB.

The thinning rate calculated from the model is ~ 5 m a^{-1} more negative than the observations over the entire domain
375 of Lugge Glacier and also the lower part of Thorthormi Glacier (Fig. 8b), which is probably due to the uncertainties in the estimated ice thickness and basal sliding conditions. Sensitivity tests demonstrate that the surface flow velocities vary by ± 10 % and ± 19 % when changing the constant sliding coefficient (C) by ± 10 % and the ice thickness by ± 10 m (Fig. S3), respectively. Changes in the emergence velocity for the same sensitivity tests are ± 7 % and ± 11 %, respectively. The two-dimensional feature is another reason for the insufficient modelled results, because the model neglects drag from the side walls and changes
380 in glacier width. The SMB uncertainty is estimated to be 11 % from thermal resistance (Fig. S1b). Nevertheless, our numerical experiments demonstrate that dynamically induced ice thickening compensates the negative SMB in the lower part of a land-terminating glacier, resulting in less ice thinning in comparison with a lake-terminating glacier. Further measurements of the spatial distributions of ice thickness and SMB will help in deriving more accurate estimates of the effect of ice dynamics on glacier thinning.

385 ## 5.3 Glacier retreat

Lugge Glacier has retreated continuously and at a nearly constant rate from 2000 to 2011 (Fig. 5). Bathymetric data suggest that glacier ice below the lake level accounted for 89 % of the full ice thickness at the calving front in 2002 (Fig. 6b). The lake level is close to the ice flotation level, where the basal water pressure equals the ice overburden pressure, suggesting that calving caused by ice flotation regulates the glacier front position (Van der Veen, 1996). Glaciers rapidly retreat by calving
390 when the lake level reaches the flotation level (e.g., Motyka et al., 2002; Tsutaki et al., 2011). Moreover, retreat is accelerated when the glacier terminus is situated on a reversed bed slope (e.g., Nick et al., 2009). A recent numerical study estimated overdeepening of Lugge Glacier within 1500 m of the 2009 terminus (Linsbauer et al., 2016), suggesting further rapid retreat in the future. Recent glacier inventories indicate that Lugge Glacier has a smaller accumulation area than Thorthormi Glacier (Nuimura et al., 2015; Nagai et al., 2016), suggesting that a sufficient ice flux cannot be supplied to the lower part of the glacier
395 to compensate for the ongoing ice thinning.

After progressive mass loss since 2000, the front of Thorthormi Glacier detached from the terminal moraine and retreated further from November 2010 to December 2011 (Fig. 4a). The glacier ice was still in contact with the moraine during the field campaign in September 2011, but the glacier was completely detached from the moraine on the 2 December 2011 Landsat 7 image. Satellite images taken after 2 December 2011 show a large number of icebergs floating in the lake, suggesting rapid
400 calving due to ice flotation. A numerical study suggested that a proglacial lake longer than a certain longitudinal length is also preferable for autonomous expansion through valley wind over the lake surface (Sakai et al., 2009). A previous study estimated that the overdeepening of Thorthormi Glacier extends for > 3000 m from the terminal moraine (Linsbauer et al., 2016), which

suggests that continued glacier thinning will lead to rapid retreat of the entire section of the terminus as the ice thickness reaches flotation.

405   Experiment 2 simulates a significant increase in surface flow velocity at the lower part of Thorthormi Glacier when a proglacial lake forms (Fig. 7e). Previous studies reported the speed up and rapid retreat of glaciers after detachment from a terminal ridge or bedrock bump (e.g., Boyce et al., 2007; Sakakibara and Sugiyama, 2014; Trüssel et al., 2015). In addition to the reduction in back stress, thinning itself decreases the effective pressure (ice overburden minus basal water pressure), which enhances basal ice motion and increases flow velocity (Sugiyama et al., 2011). A decrease in the effective pressure also

410   enhances shear stress in the water saturated till layer beneath the glacier (Cuffey and Paterson, 2010), though little information is available on subglacial sedimentation in the Himalayas. Acceleration near the terminus results in ice thinning and a decrease in effective pressure, which in turn leads to further acceleration of glacier flow (e.g., Benn et al., 2007b). Although no clear acceleration was observed during 2002–2011 (Fig. 3a), it is likely that the thinning and retreat of Thorthormi Glacier will be accelerated in the near future due to the formation and expansion of the proglacial lake.

415   **6   Conclusions**

To better understand the importance of glacial lake formation on rapid glacier thinning, we carried out field and satellite based measurements across the lake-terminating Lugge Glacier and the land-terminating Thorthormi and Lugge II glaciers in the Lunana region, Bhutan Himalaya. Surface elevations were surveyed in 2011 by differential GPS across the lower parts of the glaciers and compared with a 2004 GPS survey. The flow velocity and terminus positions of the glaciers were determined

420   from optical satellite images. We also performed numerical experiments to quantify the contributions of surface mass balance (SMB) and ice dynamics in relation to the observed ice thinning.

Lugge Glacier has experienced rapid ice thinning at an average rate of -4.67 ± 0.02 m a^{-1}, which is 3.3 times greater than that of Thorthormi Glacier, even though the SMB was less negative. The numerical modelling results, using the present glacier geometries, demonstrate that Thorthormi Glacier is subjected to a longitudinally compressive flow regime, suggesting

425   that dynamically induced thickening compensates for the negative SMB, and thus results in less ice thinning than at Lugge Glacier. Conversely, the flow of Lugge Glacier is nearly uniform along its central flowline, suggesting that the dynamically induced change in ice thickness is small, with the rapid thinning of Lugge Glacier driven by surface melt. This study reveals that contrasting ice flow regimes cause different ice thinning observations between lake- and land-terminating glaciers in the Bhutan Himalaya.

430   Lugge Glacier retreated continuously from 2000 to 2011, shrinking at a rate of 0.03 km^2 a^{-1}. The ice approaching the calving front is near flotation, suggesting that the terminus retreat will be accelerated by active calving in the future. Thorthormi Glacier has been retreating since 2000, resulting in the detachment of the glacier front from the terminal moraine and the formation of a proglacial lake in 2011. Ice flow modelling with the lake-terminating boundary condition indicates a significant increase in surface flow velocities near the calving front, which leads to continued glacier retreat. This positive feedback will be activated

435   in Thorthormi Glacier with the expansion of the proglacial lake, causing further thinning and retreat in the near future.

Data availability. The data for Figs. 1–8 are provided in Microsoft Excel format in the Supplement. The ALOS satellite data are available for purchase from the Remote Sensing Technology Center of Japan (https://www.restec.or.jp/en/). The Landsat 7 ETM+ satellite data are distributed by the United States Geological Survey (http://landsat.usgs.gov/).

Author contributions. KF and AS designed the study. KF, JK, TN, PT, and ST conducted the field survey in 2011. KF analysed the survey
440 data in 2004 and 2011, and simulated the surface mass balance. TN calculated the satellite based surface flow velocity. SS provided ice flow models. ST analysed the data. ST and KF wrote the paper, with contributions from AS and SS.

Competing interests. The authors declare that they have no conflict of interest.

Acknowledgements. We thank the Department of Geology and Mines, Bhutan, for providing the opportunity and permission to conduct the field observations. We thank S. Takenaka, M. Sano, A. Sasaki, K. Ghallay and logistic members for their support during the field campaign.
445 This research was supported by the Science and Technology Research Partnership for Sustainable Development (SATREPS) supported by the Japan Science and Technology Agency (JST) and the Japan International Cooperation Agency (JICA). Support was also provided by the Funding Program for Next Generation World Leading Researchers (NEXT Program, GR052), and JSPS-KAKENHI (grant number 26257202).

References

450   Ageta, Y., Iwata, S., Yabuki, H., Naito, N., Sakai, A., Narama, C., and Karma: Expansion of glacier lakes in recent decades in the Bhutan
       Himalayas, IAHS Publ., 264, 165–175, 2000.

Azam, M. F., Wagnon, P., Berthier, E., Vincent, C., Fujita, K., and Kargel, J. S.: Review of the status and mass changes of Himalayan-
       Karakoram glaciers, J. Glaciol., 1–14, https://doi.org/10.1017/jog.2017.86, 2018.

Bajracharya, S. R., Maharjan, S. B., and Shrestha, F.: The status and decadal change of glaciers in Bhutan from the 1980s to 2010 based on
455   satellite data, Ann. Glaciol., 55, 159–166, https://doi.org/10.3189/2014AoG66A125, 2014.

Benn D., Hulton, N. R. J., and Mottram, R. H.: 'Calving lows', 'sliding laws', and the stability of tidewater glaciers, Ann. Glaciol., 46,
       123–130, https://doi.org/10.3189/172756407782871161, 2007a.

Benn, D., Warren, C., and Mottram, R.: Calving processes and the dynamics of calving glaciers, Earth-Sci. Rev., 82, 143–179,
       https://doi.org/10.1016/j.earscirev.2007.02.002, 2007b.

460   Berthier, E., Arnaud, Y., Kumar, R., Ahmad, S., Wagnon, P., and Chevallier, P.: Remote sensing estimates of glacier mass balances in the
       Himachal Pradesh (Western Himalaya, India), Remote Sens. Environ., 108, 327–338, https://doi.org/10.1016/j.rse.2006.11.017, 2007.

Bolch, T., Pieczonka, T., and Benn, D. I.: Multi-decadal mass loss of glaciers in the Everest area (Nepal Himalaya) derived from stereo
       imagery, The Cryosphere, 5, 349–358, https://doi.org/10.5194/tc-5-349-2011, 2011.

Bolch, T., Kulkarni, A., Kääb, A., Huggel, C., Paul, F., Cogley, J. G., Frey, H., Kargel, J. S., Fujita, K., Scheel, M., Bajracharya, S., Stoffel,
465   M.: The state and fate of Himalayan Glaciers, Science, 336, 310–314, https://doi.org/10.1126/science.1215828, 2012.

Bollasina, M., Ming, Y., and Ramaswamy, V.: Anthropogenic aerosols and the weakening of the South Asian summer monsoon, Science,
       334, 502–505, https://doi.org/10.1126/science.1204994, 2011.

Boyce, E. S., Motyka, R. J., and Truffer, M.: Flotation and retreat of a lake-calving terminus, Mendenhall Glacier, southeast Alaska, USA, J.
       Glaciol., 53, 211–224, https://doi.org/10.3189/172756507782202928, 2007.

470   Brun, F., Berthier, E., Wagnon, P., Kääb, A., and Treichler, D.: A spatially resolved estimate of High Mountain Asia glacier mass balances
       from 2000 to 2016, Nat. Geosci., 10, 668–673, https://doi.org/10.1038/ngeo2999, 2017.

Carrivick, J. L., and Tweed, F. S.: Proglacial lakes: character, behaviour and geological importance, Quaternary Sci. Rev., 78, 34–52,
       https://doi.org/10.1016/j.quascirev.2013.07.028, 2013.

Cogley, J. G.: Glacier shrinkage across High Mountain Asia, Ann. Glaciol., 57, 41–49, https://doi.org/10.3189/2016AoG71A040, 2016.

475   Cuffey, K. M. and Paterson, W. S. B.: The physics of glaciers, Oxford, Butterworth-Heinemann, 2010.

Dehecq, A., Gourmelen, N., and Trouve, E.: Deriving large-scale glacier velocities from a complete satellite archive: Application to the
       Pamir–Karakoram–Himalaya, Remote Sens. Environ., 162, 55–66, https://doi.org/10.1016/j.rse.2015.01.031, 2015.

Farinotti, D., Huss, M., Bauder, A., Funk, M., and Truffer, M.: A method to estimate the ice volume and ice-thickness distribution of alpine
       glaciers, J. Glaciol., 55, 422–430, https://doi.org/10.3189/002214309788816759, 2009.

480   Fujita, K.: Effect of precipitation seasonality on climatic sensitivity of glacier mass balance, Earth Planet. Sci. Lett., 276, 14–19,
       https://doi.org/10.1016/j.epsl.2008.08.028, 2008.

Fujita, K., and Ageta, Y.: Effect of summer accumulation on glacier mass balance on the Tibetan Plateau revealed by mass-balance model, J.
       Glaciol., 46, 244–252, https://doi.org/10.3189/172756500781832945, 2000.

Fujita, K. and Nuimura, T.: Spatially heterogeneous wastage of Himalayan glaciers, P. Natl. Acad. Sci. USA, 108, 14011–14014,
485   https://doi.org/10.1073/pnas.1106242108, 2011.

Fujita, K., and Sakai, A.: Modelling runoff from a Himalayan debris-covered glacier, Hydrol. Earth Syst. Sci., 18, 2679–2694, https://doi.org/10.5194/hess-18-2679-2014, 2014.

Fujita, K., Suzuki, R., Nuimura, T., and Sakai, A.: Performance of ASTER and SRTM DEMs, and their potential for assessing glacial lakes in the Lunana region, Bhutan Himalaya, J. Glaciol., 54, 220–228, 2008.

490 Fujita, K., Sakai, A., Nuimura, T., Yamaguchi, S., and Sharma, R. R.: Recent changes in Imja Glacial Lake and its damming moraine in the Nepal Himalaya revealed by in situ surveys and multi-temporal ASTER imagery, Environ. Res. Lett., 4, 045205, https://doi.org/10.1088/1748-9326/4/4/045205, 2009.

Fujita, K., Takeuchi, N., Nikitin, S. A., Surazakov, A. B., Okamoto, S., Aizen, V. B., and Kubota, J.: Favorable climatic regime for maintaining the present-day geometry of the Gregoriev Glacier, Inner Tien Shan, The Cryosphere, 5, 539–549, https://doi.org/10.5194/tc-5-539-2011, 495 2011.

Fujita, K., Sakai, A., Takenaka, S., Nuimura, T., Surazakov, A. B., Sawagaki, T., and Yamanokuchi, T.: Potential flood volume of Himalayan glacial lakes, Nat. Hazards Earth Syst. Sci., 13, 1827–1839, https://doi.org/10.5194/nhess-13-1827-2013, 2013.

Funk, M., and Röthlisberger, H.: Forecasting the effects of a planned reservoir which will partially flood the tongue of Unteraargletscher in Switzerland, Ann. Glaciol., 13, 76–81, https://doi.org/10.1017/S0260305500007679, 1989.

500 Gardelle, J., Arnaud, Y., and Berthier, E.: Contrasted evolution of glacial lakes along the Hindu Kush Himalaya mountain range between 1990 and 2009, Global Planet. Change, 75, 47–55, https://doi.org/10.1016/j.gloplacha.2010.10.003, 2011.

Gardelle, J., Berthier, E., Arnaud, Y., and Kääb, A.: Region-wide glacier mass balances over the Pamir-Karakoram-Himalaya during 1999–2011, The Cryosphere, 7, 1263–1286, https://doi.org/10.5194/tc-7-1263-2013, 2013.

Glen, J. W.: The creep of polycrystalline ice, Proc. R. Soc. London, Sea. A, 228, 519–538, https://doi.org/10.1098/rspa.1955.0066, 1955.

505 Gudmundsson, G. H.: A three-dimensional numerical model of the confluence area of Unteraargletscher, Bernese Alps, Switzerland, J. Glaciol., 45, 219–230, https://doi.org/10.3198/1999JoG45-150-219-230, 1999.

Heid, T., and Kääb, A.: Evaluation of existing image matching methods for deriving glacier surface displacements globally from optical satellite imagery, Remote Sens. Environ., 118, 339–355, https://doi.org/10.1016/j.rse.2011.11.024, 2012.

Hewitt, H. and Liu, J.: Ice-dammed lakes and outburst floods, Karakoram Himalaya: historical perspectives on emerging threats, Physical 510 Geography, 31, 528–551, https://doi.org/10.2747/0272-3646.31.6.528, 2010.

Huss, M., and Hock, R.: A new model for global glacier change and sea-level rise, Front. Earth. Sci., 3:54, https://doi.org/10.3389/feart.2015.00054, 2015.

Immerzeel, W. W., Van Beek, L. P., and Bierkens, M. F.: Climate change will affect the Asian water towers, Science, 328, 1382–1385, https://doi.org/10.1126/science.1183188, 2010.

515 Kääb, A.: Combination of SRTM3 and repeat ASTER data for deriving alpine glacier flow velocities in the Bhutan Himalaya, Remote Sens. Environ., 94, 463–474, https://doi.org/10.1016/j.rse.2004.11.003, 2005.

Kääb, A., Berthier, E., Nuth, C., Gardelle, J., and Arnaud, Y.: Contrasting patterns of early twenty-first-century glacier mass change in the Himalayas, Nature, 488, 495–498, https://doi.org/10.1038/nature11324, 2012.

Kanamitsu, M., Ebisuzaki, W., Woollen, J., Yang, S-K., Hnilo, J. J., Fiorino, M., and Potter., G. L.: NCEP-DOE AMIP-II Reanalysis (R-2), 520 B. Am. Meteorol. Soc., 1631–1643, https://doi.org/10.1175/BAMS-83-11-1631, 2002.

King, O., Quincey, D. J., Carrivick, J. L., and Rowan, A. V.: Spatial variability in mass loss of glaciers in the Everest region, central Himalayas, between 2000 and 2015, The Cryosphere, 11, 407–426, https://doi.org/10.5194/tc-11-407-2017, 2017.

Komori, J.: Recent expansions of glacial lakes in the Bhutan Himalayas, Quatern. Int., 184, 177–186, https://doi.org/10.1016/j.quaint.2007.09.012, 2008.

525 Lamsal, D., Fujita, K., and Sakai, A.: Surface lowering of the debris-covered area of Kanchenjunga Glacier in the eastern Nepal Himalaya since 1975, as revealed by Hexagon KH-9 and ALOS satellite observations, The Cryosphere, 11, 2815–2827, https://doi.org/10.5194/tc-11-2815-2017, 2017.

Leprince, S., Barbot, S., Ayoub, F., and Avouac, J-P.: Automatic and precise orthorectification, coregistration, and subpixel correlation of satellite images, application to ground deformation measurements, IEEE Trans. Geosci. Remote Sens., 45, 1529–1558, 530 https://doi.org/10.1109/TGRS.2006.888937, 2007.

Linsbauer, A., Frey, H., Haeberli, W., Machguth, H., Azam, M., and Allen, S.: Modelling glacier-bed overdeepenings and possible future lakes for the glaciers in the Himalaya–Karakoram region, Ann. Glaciol., 57, 119–130, https://doi.org/10.3189/2016AoG71A627, 2016.

Mattson, L. E., Gardner, J. S., and Young, G. J.: Ablation on debris covered glaciers: an example from the Rakhiot Glacier, Punjab, Himalaya, IAHS Publication, 218, 289–296, 1993.

535 Maurer, J. M., Rupper, S. B., and Schaefer, J. M.: Quantifying ice loss in the eastern Himalayas since 1974 using declassified spy satellite imagery, The Cryosphere, 10, 2203–2215, https://doi.org/10.5194/tc-10-2203-2016, 2016.

Mörg, T., Maussion, F., and Scherer, D.: Mid-latitude westerlies as a driver of glacier variability in monsoonal High Asia, Nature Climate Change, 4, 68–73, https://doi.org/10.1038/nclimate2055, 2014.

Motyka, R. J., O'Neel, S., Connor, C. L., and Echelmeyer, K. A.: Twentieth century thinning of Mendenhall Glacier, Alaska, and its rela-540 tionship to climate, lake calving, and glacier runoff, Global Planet. Change, 35, 93–112, https://doi.org/10.1016/S0921-8181(02)00138-8, 2002.

Nagai, H., Fujita, K., Sakai, A., Nuimura, T., and Tadono, T.: Comparison of multiple glacier inventories with a new inventory derived from high-resolution ALOS imagery in the Bhutan Himalaya, The Cryosphere, 10, 65–85, https://doi.org/10.5194/tc-10-65-2016, 2016.

Naito, N., Suzuki, R., Komori, J., Matsuda, Y., Yamaguchi, S., Sawagaki, T., and Tshering, P.: Recent glacier shrinkages in the Lunana 545 region, Bhutan Himalayas, Global Environ. Res., 16, 13–22, 2012.

Nick, F. M., Vieli, A., Howat, I. M., and Joughin, I.: Large-scale changes in Greenland outlet glacier dynamics triggered at the terminus, Nat. Geosci., 2, 110–114, https://doi.org/10.1038/ngeo394, 2009.

Nie, Y., Sheng, Y., Liu, Q., Liu, L., Liu, S., Zhang, Y., and Song, C.: A regional-scale assessment of Himalayan glacial lake changes using satellite observations from 1990 to 2015, Remote Sens. Environ., 189, 1–13, https://doi.org/10.1016/j.rse.2016.11.008, 2017.

550 Nuimura, T., Fujita, K., Yamaguchi, S., and Sharma, R. R.: Elevation changes of glaciers revealed by multitemporal digital elevation models calibrated by GPS survey in the Khumbu region, Nepal Himalaya, 1992–2008, J. Glaciol., 58, 648–656, https://doi.org/10.3189/2012JoG11J061, 2012.

Nuimura, T., Sakai, A., Taniguchi, K., Nagai, H., Lamsal, D., Tsutaki, S., Kozawa, A., Hoshina, Y., Takenaka, S., Omiya, S., Tsunematsu, K., Tshering, P., and Fujita, K.: The GAMDAM glacier inventory: a quality-controlled inventory of Asian glaciers, The Cryosphere, 9, 555 849–864, https://doi.org/10.5194/tc-9-849-2015, 2015.

Østrem, G.: Ice melting under a thin layer of moraine and the existence of ice cores in moraine ridges, Geogr. Ann., 41, 228–230, 1959.

Sakai, A.: Glacial Lakes in the Himalayas: A Review on Formation and Expansion Processes, Global Environ. Res., 16, 23–30, 2012.

Sakai, A., and Fujita, K.: Formation conditions of supraglacial lakes on debris-covered glaciers in the Himalayas, J. Glaciol., 56, 177–181, https://doi.org/10.3189/002214310791190785, 2010.

560 Sakai, A., and Fujita, K.: Contrasting glacier responses to recent climate change in high-mountain Asia, Sci. Rep., 7, 13717, https://doi.org/10.1038/s41598-017-14256-5, 2017.

Sakai, A., Nishimura, K., Kadota, T., and Takeuchi, N.: Onset of calving at supraglacial lakes on debris covered glaciers of the Nepal Himalayas, J. Glaciol., 55, 909–917, https://doi.org/10.3189/002214309790152555, 2009.

Sakakibara, D. and Sugiyama, S.: Ice-front variations and speed changes of calving glaciers in the Southern Patagonia Icefield from 1984 to
565 2011, J. Geophys. Res.-Earth, 119, 2541–2554, https://doi.org/10.1002/2014JF003148, 2014.

Scherler, D., and Strecker, M. R.: Large surface velocity fluctuations of Biafo Glacier, central Karakoram, at high spatial and temporal resolution from optical satellite images, J. Glaciol., 58, 569–580, https://doi.org/10.3189/2012JoG11J096, 2012.

Scherler, D., Bookhagen, B., and Strecker, M. R.: Hillslope glacier coupling: The interplay of topography and glacial dynamics in High Asia, J. Geophys. Res., 116, F02019, https://doi.org/10.1029/2010JF001751, 2011.

570 Sugiyama, S., Gudmundsson, G. H., and Helbing, J.: Numerical investigation of the effects of temporal variations in basal lubrication on englacial strain-rate distribution, Ann. Glaciol., 37, 49–54, https://doi.org/10.3189/172765403781815618, 2003.

Sugiyama, S., Skvarca, P., Naito, N., Enomoto, H., Tsutaki, S., Tone, K., Marinsek, S., and Aniya, M.: Ice speed of a calving glacier modulated by small fluctuations in basal water pressure, Nat. Geosci., 4, 597–600, https://doi.org/10.1038/ngeo1218, 2011.

Sugiyama, S., Sakakibara, D., Matsuno, S., Yamaguchi, S., Matoba, S., Aoki, T.: Initial field observation on Qaanaaq ice cap, northwestern
575 Greenland, Ann. Glaciol., 55, 25–33, https://doi.org/10.3189/2014AoG66A102, 2014.

Suzuki, R., Fujita, K., and Ageta, Y.: Spatial distribution of thermal properties on debris-covered glaciers in the Himalayas derived from ASTER data, Bull. Glaciol. Res., 24, 13–22, 2007a.

Suzuki, R., Fujita, K., Ageta, Y., Naito, N., Matsuda, Y., and Karma: Meteorological observations during 2002–2004 in Lunana region, Bhutan Himalayas, Bull. Glaciol. Res., 24, 71–78, 2007b.

580 Trüssel, B. L., Motyka, R. J., Truffer, M., and Larsen, C. F.: Rapid thinning of lake-calving Yakutat Glacier and the collapse of the Yakutat Icefield, southeast Alaska, USA, J. Glaciol., 59, 149–161, https://doi.org/10.3189/2013JoG12J081, 2013.

Trüssel, B. L., Truffer, M., Hock, R., Motyka, R. J., Huss, M., and Zhang, J.: Runaway thinning of the low-elevation Yakutat Glacier, Alaska, and its sensitivity to climate change, J. Glaciol., 61, 65–75, https://doi.org/10.3189/2015JoG14J125, 2015.

Tshering, P., and Fujita, K.: First in situ record of decadal glacier mass balance (2003–2014) from the Bhutan Himalaya, Ann. Glaciol., 57,
585 289–294, https://doi.org/10.3189/2016AoG71A036, 2016.

Tsutaki, S., Nishimura, D., Yoshizawa, T., and Sugiyama, S.: Changes in glacier dynamics under the influence of proglacial lake formation in Rhonegletscher, Switzerland, Ann. Glaciol., 52, 31–36, https://doi.org/10.3189/172756411797252194, 2011.

Tsutaki, S., Sugiyama, S., Nishimura, D., and Funk, M.: Acceleration and flotation of a glacier terminus during formation of a proglacial lake in Rhonegletscher, Switzerland, J. Glaciol., 59, 559–570, https://doi.org/10.3189/2013JoG12J107, 2013.

590 Tsutaki, S., Sugiyama, S., Sakakibara, D., and Sawagaki, T.: Surface elevation changes during 2007–13 on Bowdoin and Tugto Glaciers, northwestern Greenland, J. Glaciol., 62, 1083–1092, https://doi.org/10.1017/jog.2016.106, 2016.

Van der Veen, C. J.: Tidewater calving, J. Glaciol., 42, 375–385, https://doi.org/10.1017/S0022143000004226, 1996.

Vieli, A., and Nick, F. M.: Understanding and modelling rapid dynamic changes of tidewater outlet glaciers: issues and implications, Surv. Geophys., 32, 437–458, https://doi.org/10.1007/s10712-011-9132-4, 2011.

595 Vincent, C., Wagnon, P., Shea, J. M., Immerzeel, W. W., Kraaijenbrink, P., Shrestha, D., Soruco, A., Arnaud, Y., Brun, F., Berthier, E., and Sherpa, S. F.: Reduced melt on debris-covered glaciers: investigations from Changri Nup Glacier, Nepal, The Cryosphere, 10, 1845–1858, https://doi.org/10.5194/tc-10-1845-2016, 2016.

Warren, C. R., and Kirkbride, M. P.: Calving speed and climatic sensitivity of New Zealand lake-calving glaciers, Ann. Glaciol., 36, 173–178, https://doi.org/10.3189/172756403781816446, 2003.

600 Yamada, T., Naito, N., Kohshima, S., Fushimi, H., Nakazawa, F., Segawa, T., Uetake, J., Suzuki, R., Sato, N., Karma, Chhetri, I. K., Gyenden, L., Yabuki, H., and Chikita, K.: Outline of 2002 – research activities on glaciers and glacier lakes in Lunana region, Bhutan Himalaya, Bull. Glaciol. Res., 21, 79–90, 2004.

Yao, T., Thompson, L., Yang, W., Yu, W., Gao, Y., Guo, X., Yang, X., Duan, K., Zhao, H., Xu, B., Pu, J., Lu, A., Xiang, Y. Kattel, D. B., and Joswiak, D.: Different glacier status with atmospheric circulations in Tibetan Plateau and surroundings, Nature Climate Change, 2,

605 663–667, https://doi.org/10.1038/nclimate1580, 2012.

Zhang, Y., Fujita, K., Liu, S. Y., Liu, Q., and Nuimura, T.: Distribution of debris thickness and its effect on ice melt at Hailuogou glacier, southeastern Tibetan Plateau, using in situ surveys and ASTER imagery, J. Glaciol., 57, 1147–1157, https://doi.org/10.3189/002214311798843331, 2011.

Zemp, M., Frey, H., Gärtner-Roer, I., Nussbaumer, S. U., Hoelzle, M., Paul, F., Haeberli, W., Denzinger, F., Ahlstrøm, A. P., Anderson, B.,

610 Bajracharya, S., Baroni, C., Braun, L. N., Cáceres, B. E., Casassa, G., Cobos, G., Dávila, L. R., Delgado Granados, H., Demuth, M. N., Espizua, L., Fischer, A., Fujita, K., Gadek, B., Ghazanfar, A., Hagen, J. O., Holmlund, P., Karimi, N., Li, Z. Q., Pelto, M., Pitte, P., Popovnin, V. V., Portocarrero, C. A., Prinz, R., Sangewar, C. V., Severskiy, I., Sigurðsson, O., Soruco, A., Usubaliev, R., and Vincent, C.: Historically unprecedented global glacier decline in the early 21st century, J. Glaciol., 61, 745–761, https://doi.org/10.3189/2015JoG15J017, 2015.

Table 1. Observed elevation changes (*dh*) and rate of elevation changes (*dh/dt*), with standard errors on and off glaciers, in the Lunana region, Bhutan Himalaya, during 2004–2011. The simulated surface mass balance (SMB), emergence velocity (v_e), and rate of elevation change are also indicated, along with observed number of 1 m DEM grid points (*n*).

Glacier	n	Observed *dh* (m)	Observed *dh/dt* (m a^{-1})	SMB (m w.e. a^{-1})	v_e (m w.e. a^{-1})	Simulated *dh/dt* (m a^{-1})
Thorthormi	431	-9.79 ± 0.09	-1.40 ± 0.01	-7.87 ± 1.46	0.27 ± 2.62	-8.44 ± 4.08
Lugge	248	-32.70 ± 0.12	-4.67 ± 0.02	-5.98 ± 1.11	-2.18 ± 2.62	-9.07 ± 3.73
Lugge II	258	-4.43 ± 0.12	-0.63 ± 0.02	-4.38 ± 0.49		
Off glacier	3893	0.48 ± 0.03				
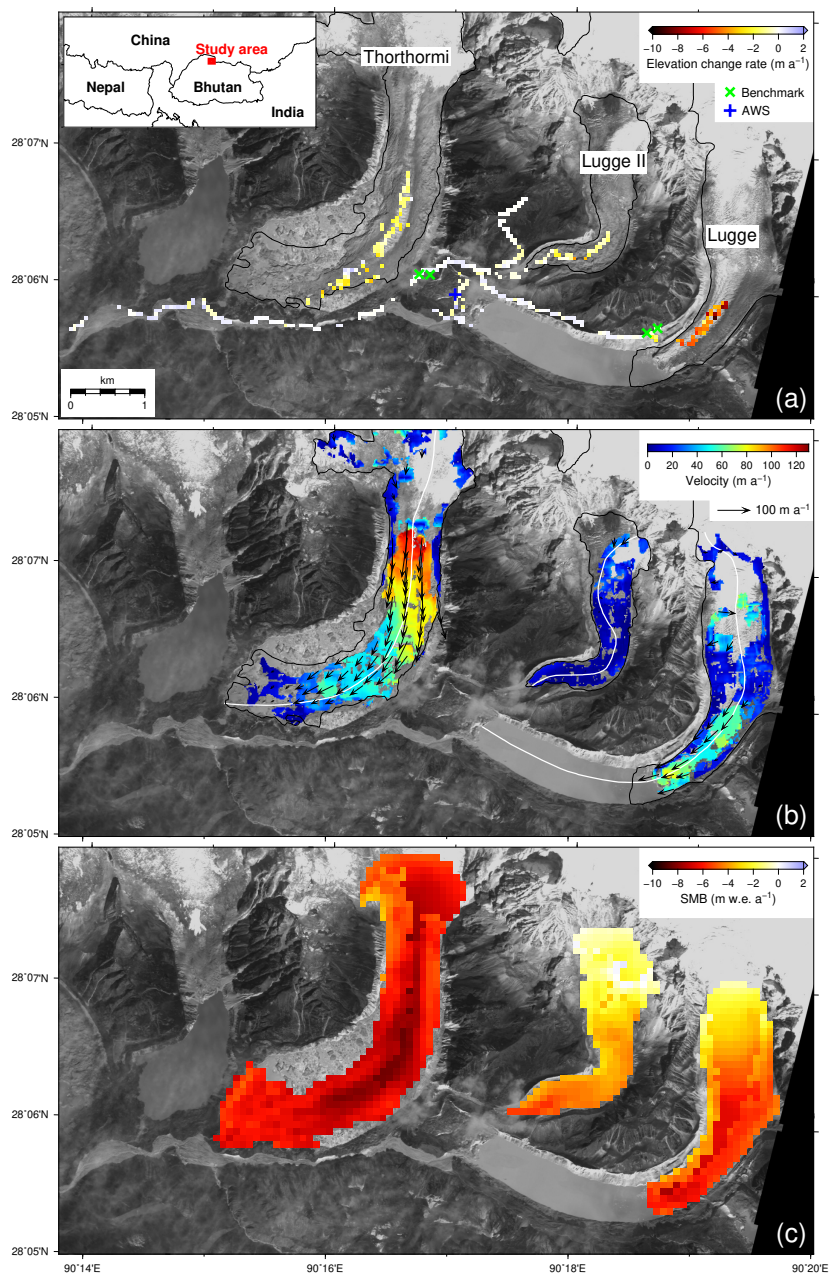
Figure 1. Glaciers and glacial lakes in the Lunana region, Bhutan Himalaya, superimposed with (a) the rate of elevation change for the 2004–2011 period, (b) surface flow velocities (arrows) with magnitude (colour scale), between 30 January 2007 and 1 January 2008, and (c) simulated surface mass balance (SMB) for the 2002–2004 period. The inset in (a) shows the location of the study site. The rate of elevation change in (a) is depicted on a 50 m grid, which is averaged from the differentiated 1 m DEMs. The light green crosses are the benchmark locations used for the GPS surveys in 2004 and 2011. The blue cross is the location of the automatic weather station installed in 2002 (Yamada et al., 2004). The black lines indicate the outline of the glaciers in November 2002. The background image is an ALOS PRISM scene from 2 December 2009. The white lines in (b) indicate the central flowline of each glacier, which is used for Figs. 3 and 6–8.
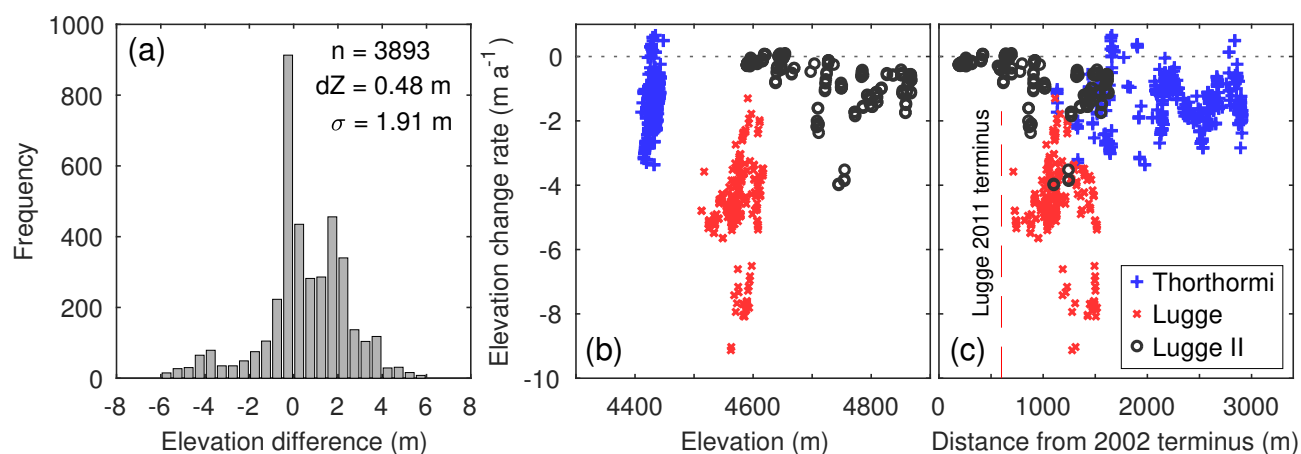
Figure 2. (a) Histogram of the elevation differences across off glacier at 0.5 m elevation bins. The rate of elevation change for Thorthormi (blue), Lugge (red) and Lugge II (black) glaciers is compared with (b) elevation in 2011, and (c) distance from the glacier terminus in 2002 along the central flowlines (Fig. 1b). the red dashed line in (c) denotes the location of the calving front of Lugge Glacier in 2011.
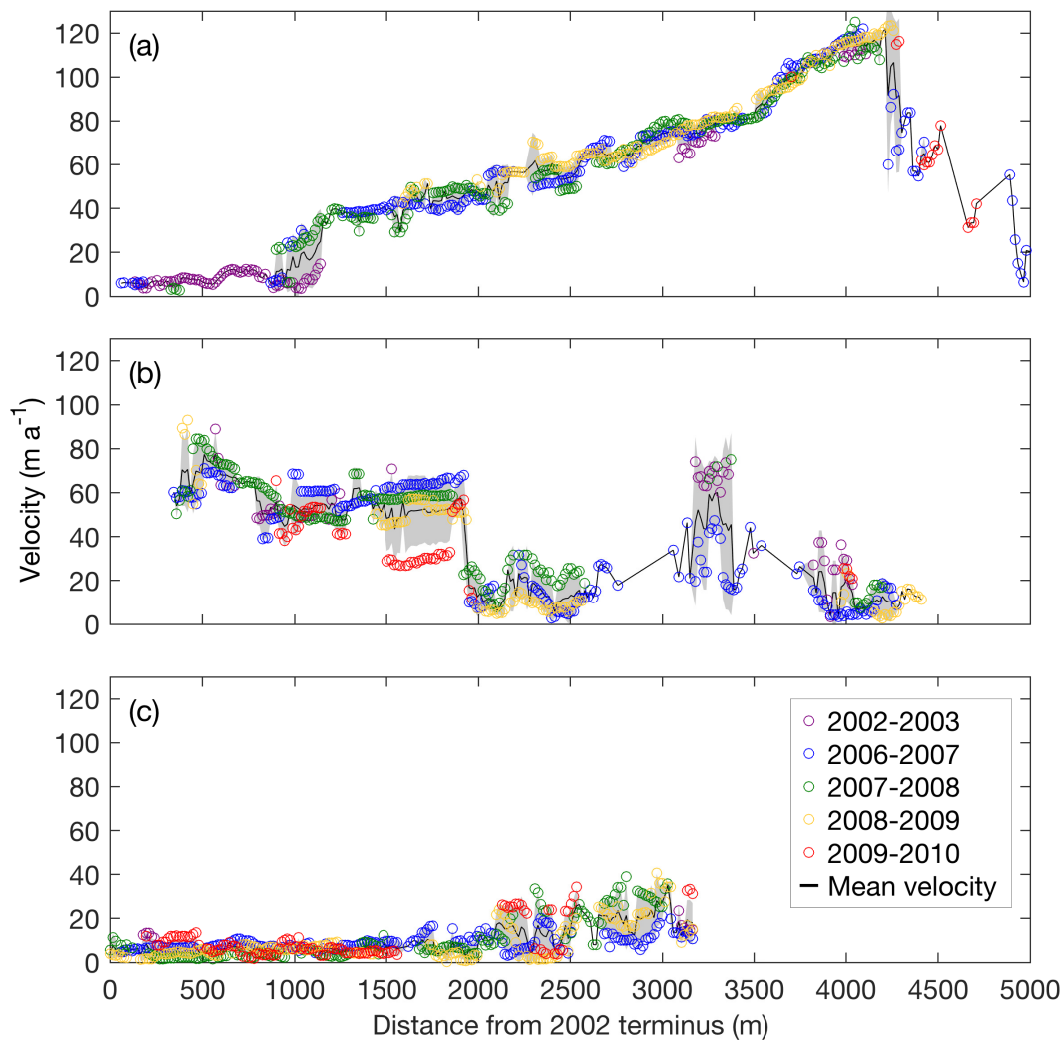
Figure 3. Surface flow velocity along the central flowlines of (a) Thorthormi, (b) Lugge and (c) Lugge II glaciers for the 2002–2010 study period. The black lines are the mean velocities from 2002 to 2010, with shaded gray regions denoting the standard deviation. The distance from each respective 2002 glacier terminus is indicated on the horizontal axis.
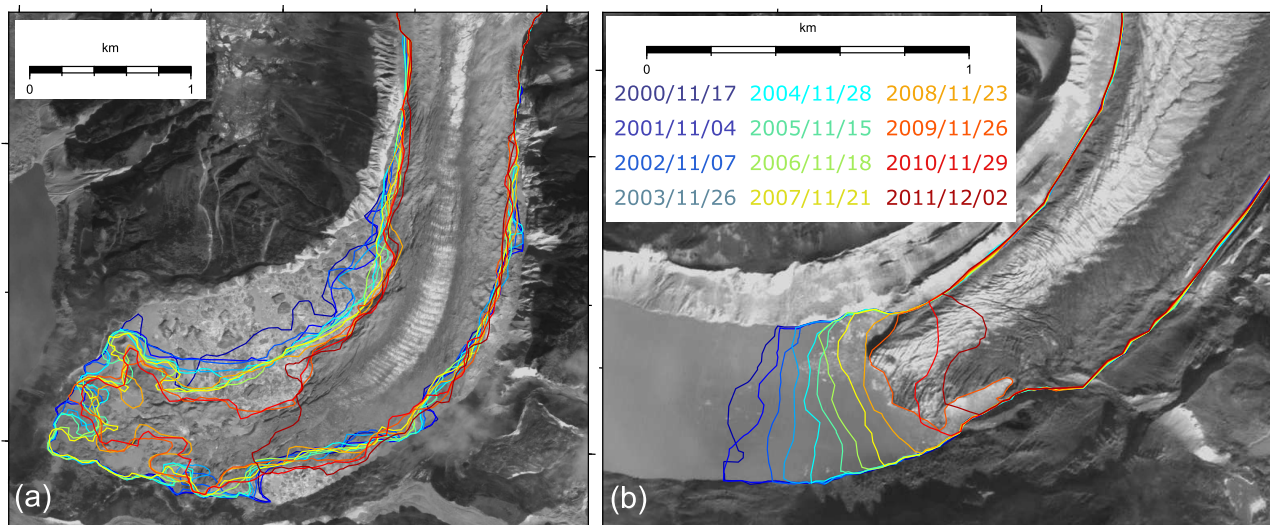
Figure 4. Glacier boundaries in the lower parts of (a) Thorthormi and (b) Lugge glaciers from 2000 to 2011. The background image is an ALOS PRISM image acquired on 2 December 2009.
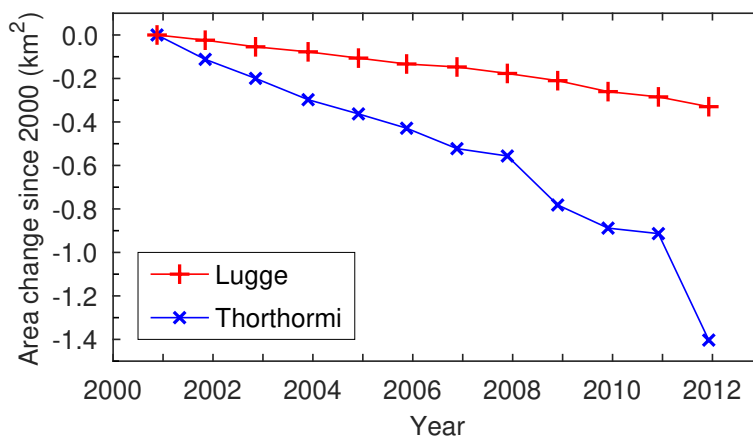
Figure 5. Cumulative area changes of Thorthormi (blue) and Lugge (red) glaciers since 17 November 2000.
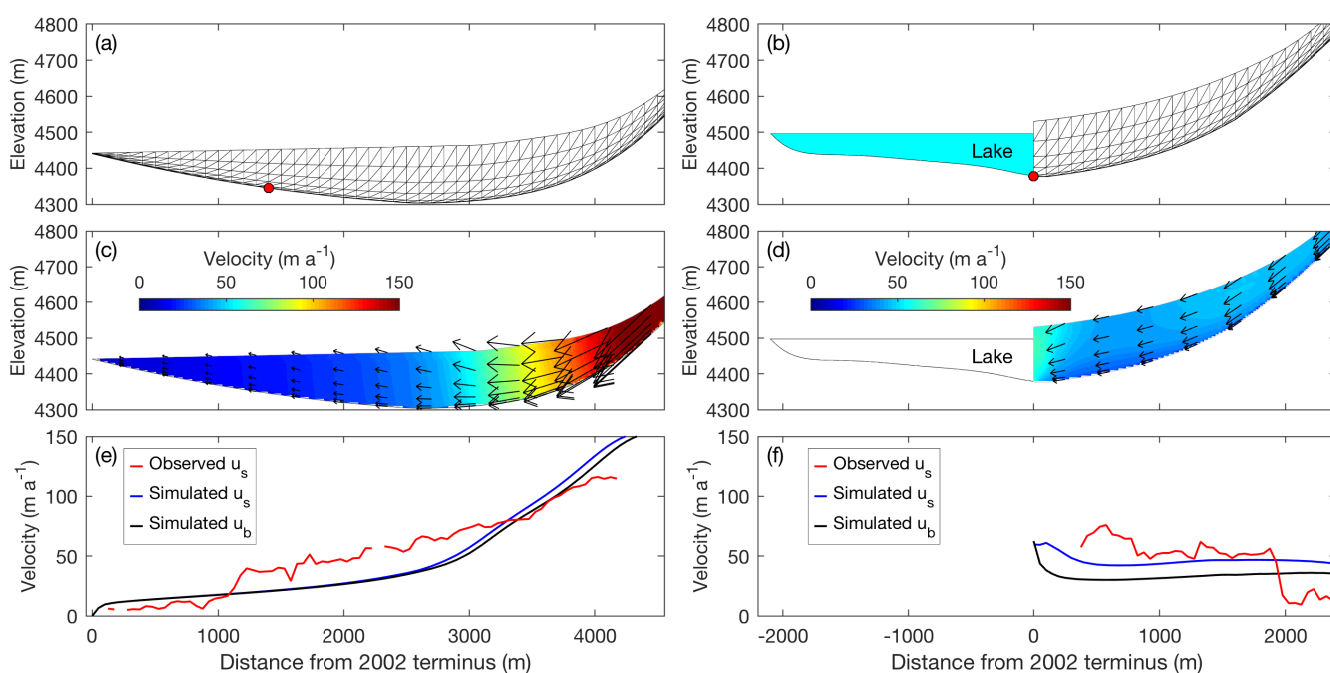
Figure 6. Ice flow simulations in longitudinal cross sections of Thorthormi (left panels) and Lugge (right panels) glaciers, with the present geometries of the glaciers employed in the models. (a and b) Finite element meshes used for the simulations, with red markers indicating the bedrock elevation based on a bathymetric survey. The light blue shading in (b) indicates Lugge Glacial Lake. Simulated (c and d) two-dimensional flow vectors (magnitude and direction) and (e and f) horizontal components of the flow velocity. The blue and black curves are the simulated surface (u_s) and basal velocities (u_b), respectively. The red curves are the observed surface velocities for 2002–2010.
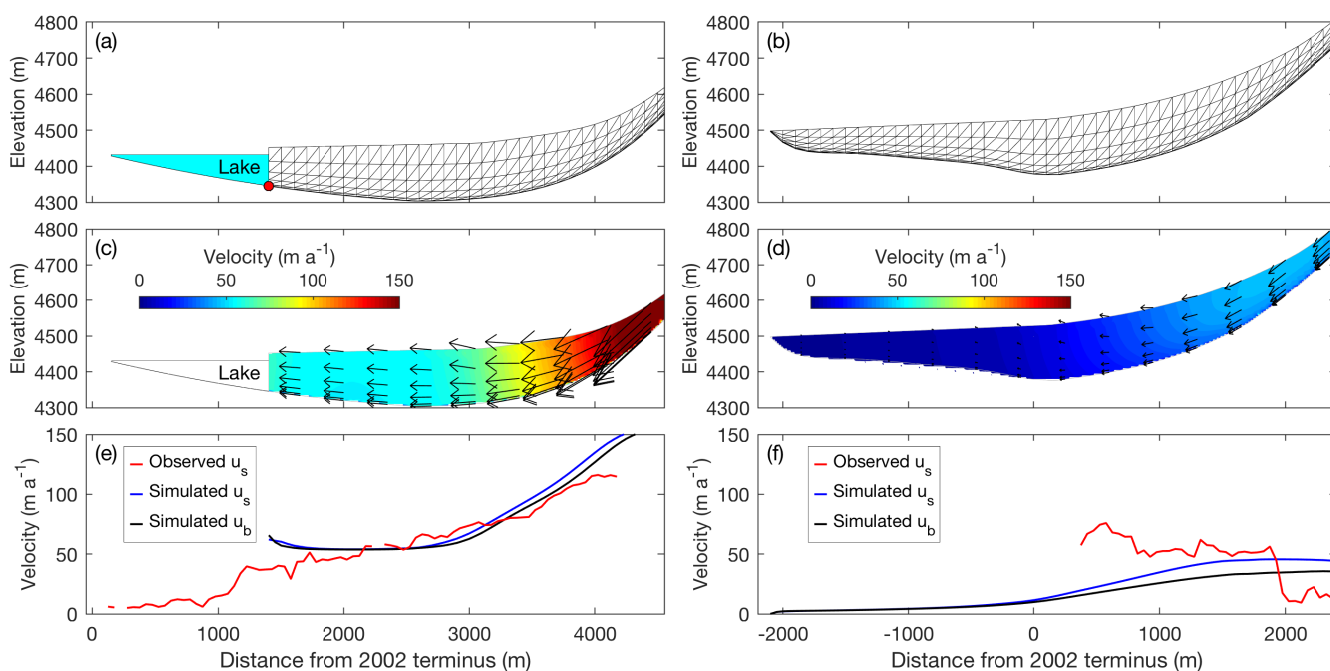
Figure 7. Ice flow simulations in longitudinal cross sections of Thorthormi Glacier under the lake-terminating condition (left panels), and Lugge Glacier under the land-terminating condition (right panels). (a and b) Finite element meshes used for the simulation. The light blue shading in (a) indicates the proglacial lake in front of Thorthormi Glacier. Simulated (c and d) two-dimensional flow vectors (magnitude and direction) and (e and f) horizontal components of the flow velocity. The blue and black curves are the simulated surface (u_s) and basal velocities (u_b), respectively. The red curves are the observed surface velocities for 2002–2010.
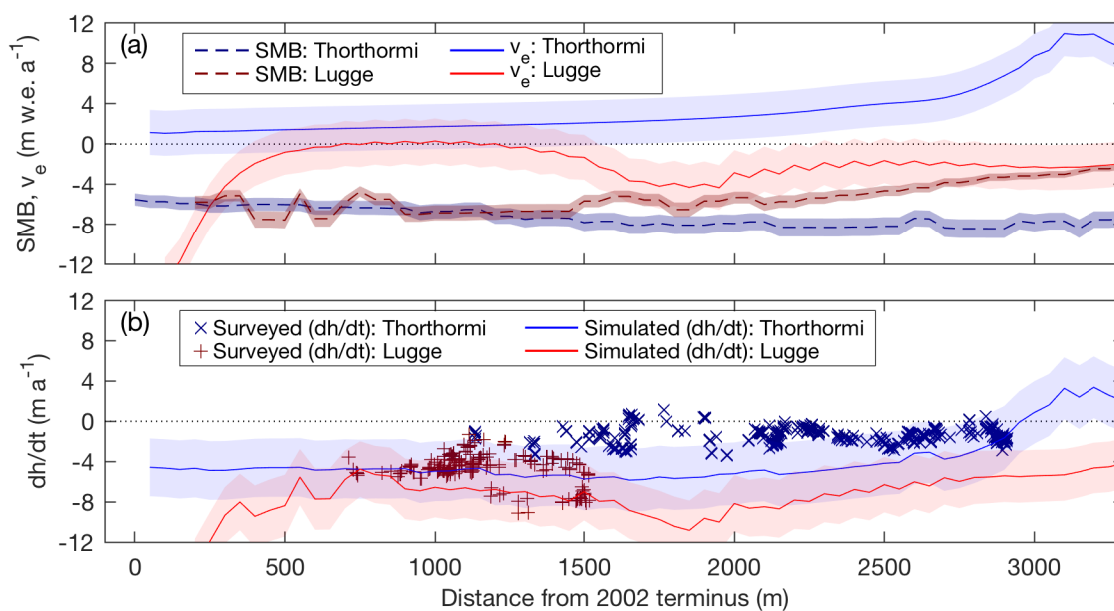
Figure 8. (a) Simulated surface mass balance (SMB) and emergence velocity (v_e) calculations along the central flowlines of Thorthormi and Lugge glaciers. (b) Rate of elevation change (*dh/dt*), as determined from differential GPS surveys during 2004–2011 (marks) and model simulations (lines). Shaded regions denote the model uncertainties for each calculation.